International Journal of Nanomedicine

Dovepress
open access to scientific and medical research

Open Access Full Text Article

ORIGINAL RESEARCH

iRGD Tumor-Penetrating Peptide-Modified Nano-Delivery System Based on a Marine Sulfated Polysaccharide for Enhanced Anti-Tumor Efficiency Against Breast Cancer

Bowei Chen[1,*], Xiaohong Liu[1,*], Yunan Li[1], Tianhe Shan[1], Liya Bai[1], Chunyu Li[2], Yinsong Wang[1]

[1]School of Pharmacy, Tianjin Key Laboratory on Technologies Enabling Development of Clinical Therapeutics and Diagnostics (Theranostics), Tianjin Medical University, Tianjin, 300070, People's Republic of China; [2]Department of Integrated Traditional Chinese and Western Medicine, International Medical School, Tianjin Medical University, Tianjin, 300070, People's Republic of China

*These authors contributed equally to this work

Correspondence: Yinsong Wang; Chunyu Li, Email wangyinsong@tmu.edu.cn; lichunyu@tmu.edu.cn

Background: Breast cancer is a common malignancy in women. Conventional clinical therapies for breast cancer all display moderate clinical efficacies and limitations. It is urgent to explore the novel and combined therapeutic strategies for breast cancer to meet clinical demand.

Methods: An iRGD tumor-penetrating peptide-modified nano-delivery system (denoted as iRGD-PSS@PBAE@JQ1/ORI nanoparticles) based on a marine sulfated polysaccharide was developed by codelivery of JQ1 (BET inhibitor) and oridonin (ORI, bioactive diterpenoid derived from traditional Chinese medicine herb). The iRGD-PSS@PBAE@JQ1/ORI NPs, surface modified with iRGD peptide conjugated propylene glycol alginate sodium sulfate (iRGD-PSS). The antitumor efficacy was evaluated both in vitro and in vivo.

Results: The prepared iRGD-PSS@PBAE@JQ1/ORI NPs effectively enhanced the tumor targeting and cellular internalization of JQ1 and ORI. Thus, JQ1 exerted the reversal effect on immune tolerance by decreasing the expression of PD-L1, while ORI displayed multiple antitumor effects, such as antiproliferation, inhibition of intracellular ROS production and inhibition of lactic acid secretion.

Conclusion: Our data revealed that iRGD peptide could significantly improve the cellular internalization and tumor penetration of the nano-delivery system. The combination of JQ1 and ORI could exert synergistic antitumor activities. Taken together, this study provides a multifunctional nanotherapeutic system to enhance the anti-tumor efficiency against breast cancer.

Keywords: iRGD peptide-modified nano-delivery system, marine sulfated polysaccharide, JQ1, oridonin, synergistic antitumor activity, breast cancer

Introduction

Breast cancer is the most malignancy in women worldwide and the second leading cause of cancer-related death in women.[1–3] Current clinical therapeutic strategies display moderate clinical efficacies and limitations, such as post-operative recurrence, chemoresistance, poor responses, and toxic side effects.[4,5] Consequently, it is an imperative task to explore the novel and combined treatment strategies for enhancing therapeutic outcomes of breast cancer.

Recently, natural products have received considerable attention due to their efficacy and safety. Propylene glycol alginate sodium sulfate (PSS) is a marine sulfated polysaccharide derivative that is used to prevent and treat ischemic cardio-cerebrovascular diseases and hyperlipidemia in China for almost 30 years.[6–8] Several studies have reported that PSS can inhibit cancer cell metastasis in vitro through inhibition of angiogenesis and platelet activation.[6,9] Accumulating evidence suggests that PSS is an ideal carrier material for selective loading or efficient co-loading of small molecules and

Received: 12 October 2021
Accepted: 13 January 2022
Published: 9 February 2022

even nanoparticles due to its favorable physical and chemical properties.[10] However, a critical obstacle of cancer treatment is the inefficient delivery of therapeutic agents due to the high spatiotemporally heterogeneous in the complicated and dense tumor stroma. Although nanotechnology-based drug delivery systems could enhance the tumor-targeted ability passively via enhanced permeability and retention (EPR) effect, growing evidences showed that the drug penetration and accumulation in tumor tissues still need improvement.[11,12] iRGD peptide (internalizing RGD) is a tumor homing and tissue penetrating peptide that possesses a specific binding ability to integrin receptors $\alpha_v\beta_3$ and $\alpha_v\beta_5$, which are overexpressed in tumor cells.[13,14] After cleaved by a protease, the C-terminal rule (C and R) motif exposes and consequently binds to the neuropilin-1 (NRP-1) receptor, which could mediate the trans-tissue and transcytosis transport pathway.[15] Many reports have verified that a nano-delivery system, either co-administrated with iRGD or in a covalent coupling way, could enhance its capability of active tumor targeting and tissue penetration, resulting in increased treatment efficacy.[16–18] Because of the above-mentioned facts, we hypothesized that PSS modified with iRGD (iRGD-PSS) could be a safe and effective tumor-targeted delivery carrier.

In this study, we synthesized a multitarget nano-delivery system iRGD-PSS@PBAE@JQ1/ORI nanoparticles (NPs) based on iRGD-PSS that co-load JQ1 and oridonin (ORI) for enhanced anti-tumor efficiency against breast cancer. JQ1 is a bromodomain and extra-terminal (BET) inhibitor that could effectively decrease the expression of PD-L1 on the tumor cell surface via reducing the c-MYC transcription, thus blocking the PD-1/PD-L1 interaction.[19–23] Furthermore, JQ1 also shows strong anti-proliferative activity against tumor cells.[24,25] ORI, a bioactive diterpenoid derived from traditional Chinese medicine herb *Rabdosia rubescens*, exhibits potent anti-cancer activities against a variety of tumor cells.[26] In addition, disulfide-containing poly (β-amino ester) (ssPBAE) which possesses pH and redox dual responsiveness was used as carrier material to prepare this nano-delivery system. Furthermore, these NPs were further surface-modified with iRGD-PSS to enhance tumor penetration and shield the positive charges of ssPBAE. As shown in Scheme 1A, this nanotherapeutic system is composed of hydrophobic ssPBAE nanocore co-loaded JQ1 and ORI, with hydrophilic iRGD-PSS nanoshell. As shown in Scheme 1B, iRGD-PSS @PBAE@JQ1/ORI NPs could reach and penetrate tumor tissue and then internalize into breast cancer cells via endocytosis mediated by iRGD and integrin receptors $\alpha_v\beta_3$ binding. Then, the iRGD-PSS@PBAE@JQ1/ORI NPs escape from acidic endosomes into the cytoplasm via the "proton sponge" effect of ssPBAE. Under the high concentration of intracellular glutathione (GSH), iRGD-PSS@PBAE@JQ1/ORI NPs will be disintegrated through the cleavage of disulfide bonds in ssPBAE. Thus, JQ1 exerts the reversal effect on immune tolerance by decreasing immune checkpoint molecule PD-L1 expression. Meanwhile, ORI exerts multiple anti-cancer activities, such as inhibition of proliferation, and lactic acid secretion, reactive oxygen species (ROS) generation, induction of cell cycle arrest, and so on.[27–30] Therefore, ORI could solidify the anti-cancer activity of JQ1, thus exerting synergistic anti-tumor activities in vitro and in vivo. Taken together, iRGD-PSS @PBAE@JQ1/ORI NPs can be used as a tumor-targeted therapeutic system for synergistic treatment against breast cancer.

Materials and Methods

Materials and Chemicals

JQ1 (≥98% purity, CAS No. 1268524-70-4) and Oridonin (>98% purity, CAS No. 28957-04-2) were purchased from Meilunbio (Dalian, China). Tumor-penetrating peptide iRGD (internalizing RGD, ≥98% purity, CRGDKGPDC) was constructed by ChinaPeptides (Shanghai, China). PSS (20 kDa) was provided by Ocean University of China (Qingdao, China). ssPBAE was synthesized according to our previous report.[31] 1-(3-dimethylaminoprophyl)-3-ethylcarbodiimide hydrochloride (EDC·HCl) and N-hydroxysuccinimide (NHS) were provided by J&K Scientific (Beijing, China). IR780 iodide, polyvinylpyrrolidone (PVP, K-30), thiazolyl blue tetrazolium bromide (MTT), 4′6-diamidino-2'-phenylindole dihydrochloride (DAPI) and 2,7-dichlorodihydrofluorescein diacetate (DCFH-DA) were obtained from Sigma Aldrich (St Louis, USA). Singlet oxygen sensor green (SOSG) and LIVE/DEAD cell staining kit were purchased from Thermo Fisher Scientific (Hudson, NH, USA). L-Lactic acid and lipopolysaccharides (LPS) were obtained from Solarbio (Beijing, China). Anti-calreticulin/AF488 antibody was purchased from Biosynthesis Biotechnology (Beijing, China). Antibodies against PD-L1, GAPDH and HRP-conjugated antibodies were provided by Bioss Antibodies (Boston, MA, USA). The FITC-labeled anti-CD86 antibody, APC-labeled anti-CD80 antibody and antibody against Ki67 were obtained from Abcam (Cambridge, UK).

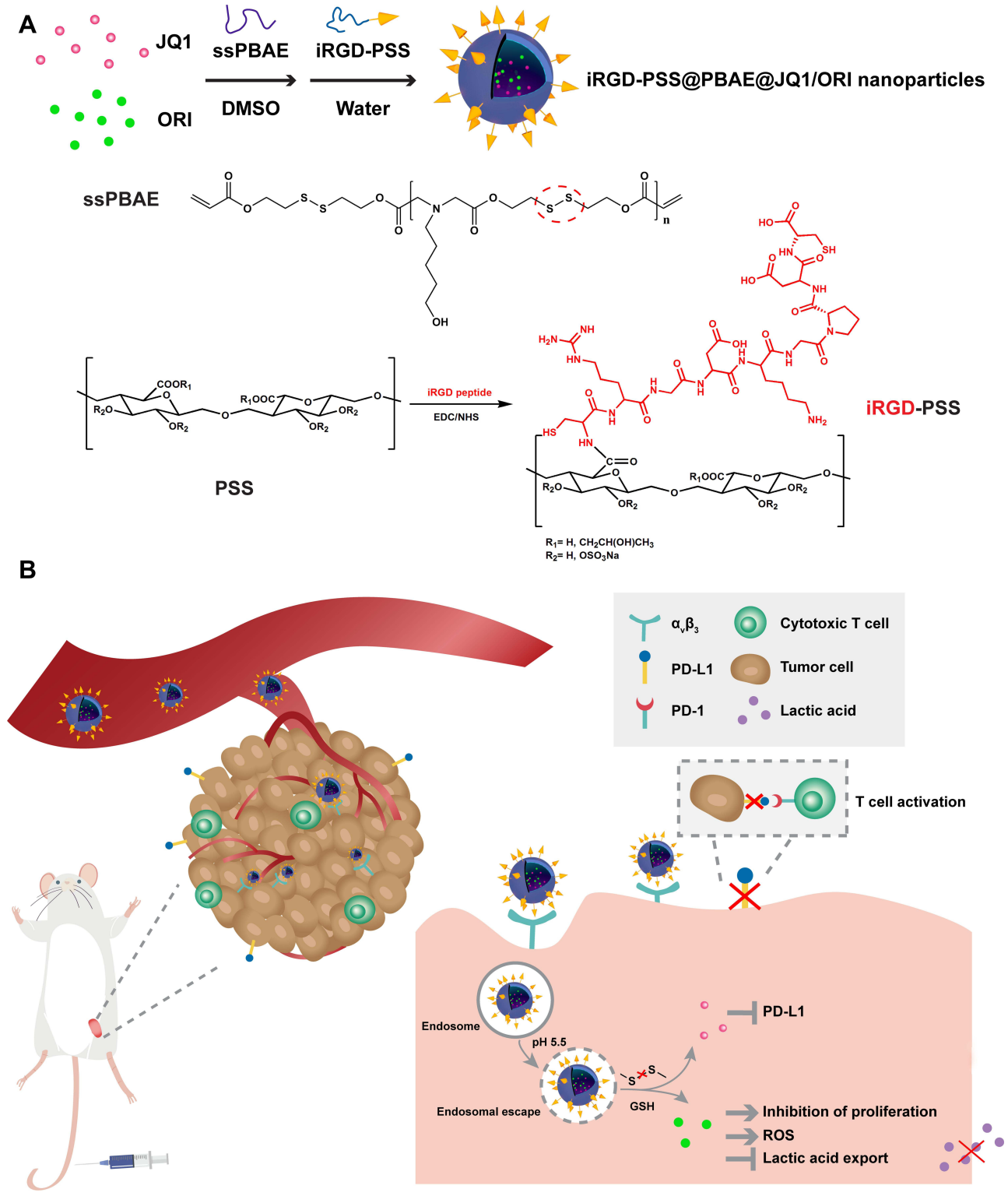

Scheme 1 Schematic diagram for preparation of iRGD-PSS@PBAE@JQ1/ORI NPs by nanoprecipitation method (**A**) and iRGD-PSS@PBAE@JQ1/ORI NPs synergistic mechanisms against breast cancer (**B**).

Cells and Animals

4T1 (mouse breast cancer cell lines) was purchased from BioVector NTCC (Beijing, China) and cultured in DMEM supplemented with 10% FBS and 1% penicillin/streptomycin. The bone marrow-derived dendritic cells (BMDCs) were

prepared according to a method previously reported.[32] BALB/c mice (female, 5–6 weeks old) were obtained from Vital River Laboratory Animal Technology Co., Ltd. (Beijing, China). For the mouse model of breast cancer, 4T1 cells (5.0×10^5) suspended in PBS were subcutaneously injected into the right groin of each mouse. All animal experiments were carried out according to the protocols approved by the Animal Care and Use Committee of Tianjin Medical University (the Laboratory Animal Use Permit Number: SYXK 2019-0004) and carried out to the NIH guide for care and use of laboratory animals.

Synthesis and Characterization of iRGD-PSS

iRGD conjugated PSS (iRGD-PSS) was synthesized by amidation reaction between the carboxyl group of PSS and terminal amino groups of iRGD in the presence of EDC and NHS. 30 mg PSS was firstly reacted with EDC (4.77 mg) and NHS (2.86 mg) in DDW (2 mL) for 2 h. Next, iRGD (7.8 mg) was added to the above solution under stirring for 48 h. Then, the mixture was purified by dialysis against deionized water and finally freeze-dried to obtain iRGD-PSS powder. The chemical structures of iRGD-PSS were confirmed by the Fourier transform infrared (FT-IR) and proton nuclear magnetic resonance spectroscopy (^{1}H-NMR) on an FT-IR spectrometer (NEXUS 470, Nicolet, USA) and an AVANCE III NMR spectrometer (400 MHz, Bruker, Germany), respectively.

Additionally, the percentage content of nitrogen in iRGD-PSS was measured by a UNICUBE elemental analyzer (Germany), and the graft efficiency of iRGD-PSS was calculated according to the following formulas: Graft efficiency (%) = (mass of grafted iRGD peptide/mass of iRGD-PSS) × 100%.

Preparation and Characterization of iRGD-PSS@PBAE@JQ1/ORI NPs

To prepare the iRGD-PSS@PBAE@JQ1/ORI NPs, a modified facile nanoprecipitation method was conducted. Briefly, JQ1 (2 mg), ORI (2 mg) and ssPBAE (12 mg) were mixed in DMSO (280 μL) under stirring for 2 h, and then the mixture was added dropwise into an aqueous solution (4 mL) containing iRGD-PSS (7 mg) and PVP (1 mg) under stirring for 2 h. Then, the above emulsion was dialyzed in deionized water, thus resulting in the iRGD-PSS@PBAE@JQ1/ORI nanoparticle dispersion. For further investigating the function of iRGD in the following experiments, PSS@PBAE@JQ1/ORI NPs were also prepared using the same method by only replacing iRGD-PSS with PSS solution. In addition, we also used IR780 as a fluorescent probe to determine the intracellular uptake and penetrating effect of NPs. As a result, IR780 encapsulated NPs named PSS@PBAE@IR780 and iRGD-PSS@PBAE@IR780 were prepared using the same method of PSS@PBAE@JQ1/ORI and iRGD-PSS@PBAE@JQ1/ORI NPs only replacing JQ1 and ORI with IR780. iRGD-PSS@PBAE@JQ1/ORI NPs were morphologically characterized by an HT7700 HITACHI transmission electron microscope (TEM, Japan), and the sizes, polydispersity indexes (PDIs) and zeta potentials were determined by a zeta and size detector (Malvern, UK). The stabilities of iRGD-PSS@PBAE@JQ1/ORI NPs were detected through monitoring their size changes during 6-day storage at 4°C. The loading contents and encapsulation efficiencies of JQ1 and ORI in iRGD-PSS@PBAE@JQ1/ORI NPs were detected by HPLC method. Due to the pH and redox responsiveness of ssPBAE, the release of JQ1 and ORI from iRGD-PSS@PBAE@JQ1/ORI NPs was measured in PBS solutions at different pH values and with/without 10 mM DTT by a dynamic dialysis method.

Cellular Internalization of IR780 Encapsulated NPs

Briefly, the cells were seeded into 12-well glass slips and further pre-incubated with 500 μM free iRGD for 2 h to bind to specific receptors. Then, these cells were further incubated separately with free IR780, PSS@PBAE@IR780 NPs and iRGD-PSS@PBAE@IR780 NPs. The concentrations of IR780 were 2 μg/mL. After incubation for 2 h, the cells were fixed with 4% paraformaldehyde, and the nuclei were stained with DAPI for 10 min. Finally, the glass slips were imaged by a confocal microscope (FV-1000, Olympus, Tokyo, Japan). Besides that, the cells were digested with trypsin, collected with PBS, and then analyzed with a flow cytometer (Accuri C6, BD Biosciences, USA) for quantitatively detecting the cellular uptake of NPs by 4T1 cells.

Penetration of IR780 Encapsulated NPs into Breast Tumor-Like Spheroids

To evaluate the tumor penetrating ability of NPs in vitro, three-dimensional spheroids of breast cancer 4T1 cells were constructed according to our lab's previously reported method.[33] In brief, a serum-free DMEM containing 1.5% agarose was added into the 96-well plates and then cooled to form the coating layers at 4°C for 30 min. 4T1 cells dispersed in DMEM containing 2.5% BD matrigel were seeded into the above 96-well plates with a density of 1×10^4 cells/well, and then the cells were cultured to form spheroids. Upon the size of spheroids was approximately 400 μm, the cells were incubated with free IR780, PSS@PBAE@IR780 and iRGD-PSS@PBAE@IR780 NPs at an equivalent IR780 concentration (15 μg/mL), respectively. For observing the distributions of IR780 fluorescence, the images of spheroids were taken by confocal microscopy at designated time intervals (2, 6, 12 h).

Cytotoxicity of iRGD-PSS@PBAE@JQ1/ORI NPs

The cytotoxicity of iRGD-PSS@PBAE@JQ1/ORI NPs was determined by MTT assay. In brief, the cells were seeded in 96-well plates at a density of 5.0×10^3 cells/well and then incubated with free JQ1, free ORI, PSS@PBAE@JQ1/ORI and iRGD-PSS@PBAE@JQ1/ORI NPs at different drug concentrations, respectively. After 24/48-hour incubation, these cells were treated with MTT solution, and the absorbance of each well was measured using a microplate reader (BioTek, USA) at 490 nm. Additionally, the combination index (CI) value of iRGD-PSS@PBAE@JQ1/ORI NPs mediated synergistic effects of JQ1 and ORI was calculated according to the following calculation formula. CI value <1, =1 and >1 represent synergism, additivity and antagonism, respectively. CI = IC_{50} of JQ1 in iRGD-PSS@PBAE@JQ1/ORI NPs/IC_{50} of free JQ1 + IC_{50} of ORI in iRGD-PSS@PBAE@JQ1/ORI NPs/IC_{50} of free ORI.

To assess the cytotoxicity of iRGD-PSS@PBAE@JQ1/ORI NPs more visibly, the LIVE/DEAD cell staining kit was used to process the above-treated cells. The live and dead cells were stained with calcein-AM and propidium iodide (PI) and finally imaged by Carl Zeiss fluorescent inverted microscope (Germany).

Cell Apoptosis Analysis

The cells were seeded in 12-well plates at a density of 1.0×10^5 cells/well and incubated separately with free JQ1, free ORI, JQ1/ORI mixture, PSS@PBAE@JQ1/ORI and iRGD-PSS@PBAE@JQ1/ORI NPs for 24 h at the JQ1 and ORI concentrations of 1.5 μg/mL. Afterward, the cells were stained with an Annexin-V-FITC/7-AAD apoptosis detection kit (BD Biosciences, USA) and finally analyzed by a flow cytometry.

Evaluation of Intracellular ROS Production

To evaluate the intracellular generation of ROS, DCFH-DA as a fluorescent probe was used to process the treated cells according to our previously reported method.[34] In brief, 4T1 cells were seeded into 12-well plates with a density of 8.0×10^4 cells/well and then incubated with free JQ1, free ORI, JQ1/ORI mixture, PSS@PBAE@JQ1/ORI and iRGD-PSS @PBAE@JQ1/ORI NPs for 24 h, respectively. Afterward, all the cells were stained with DCFH-DA. To observe the ROS intracellular locations, the cells were stained with DAPI and finally imaged by a confocal microscopy. For quantitative detection of ROS, all the cells were analyzed by a flow cytometer.

Calreticulin (CRT) Analysis

The exposure of CRT to plasma membranes of cancer cells serves as "eat me" signal to the antigen presentation cells such as DCs. Hence, we used immunofluorescence technique to evaluate the exposure levels of CRT. Briefly, the cells were seeded in 12-well plates with a density of 1.0×10^5 cells/well and then incubated with various treatments as described above for 24 h. Afterwards, all the cells were stained with anti-calreticulin/AF488 antibody (Biosynthesis Biotech, China) and then analyzed using a flow cytometer, as well as observed under a confocal microscope after DAPI staining.

Measurement of Lactic Acid Secretion

Lactic Acid assay kit (Jiancheng Bioengineering Institute, Nanjing, China) was applied to measure the levels of lactic acid secretion from 4T1 cells after various treatments. In brief, 4T1 cells were seeded separately into 12-well plates with a density of 1.0×10^5 cells/well and then incubated with various treatments as described above for 24 h. After incubation, the supernatants of each well were collected and detected using a lactic acid assay kit and then the absorbance in each well was measured at 530 nm by UV-Vis spectrophotometer.

Evaluation of Dendritic Cells Activation

We measured the expressions of costimulatory molecules CD80 and CD86 of BMDCs to evaluate the maturation of BMDCs in vitro. Briefly, BMDCs (1.0×10^6 cells/mL) were cultured with different concentrations of lactic acid (15 mM and 25 mM), as well as lipopolysaccharide (LPS, 36 μg/mL) as a positive control, respectively. After 24-hour incubation, BMDCs were stained with FITC-labeled anti-CD86 antibody (Abcam, Cambridge, UK) and APC-labeled anti-CD80 antibody (Abcam, Cambridge, UK), and subsequently analyzed by a flow cytometer. The percentage of cells staining positive for each surface protein was recorded.

Western Blotting Analysis

Western blotting analysis was conducted to assess the protein expressions of PD-L1 of tumor cells treated with free JQ1, free ORI, JQ1/ORI mixture, PSS@PBAE@JQ1/ORI and iRGD-PSS@PBAE@JQ1/ORI NPs, at the concentrations of JQ1 and ORI were approximately 1.5 μg/mL, respectively. Afterward, 4T1 cells were lysed in SDS buffer containing protease inhibitors. Then, the cell lysates were separated and transferred onto polyvinylidene difluoride (PVDF) membranes (Millipore, USA). After blocking in 5% skim milk, the membranes were incubated with primary antibodies against PD-L1 (Bioss Antibodies, USA) and GAPDH (Bioss Antibodies, USA), and then processed with the secondary antibodies (Bioss Antibodies, USA) conjugated with horseradish peroxidase (HRP). Finally, the membranes were visualized by ECL solution (Millipore, USA) and were photographed by G-BOX (Gene Company Ltd, China). Bands were analyzed using Image-Pro Plus 6.0 software (Media Cybernetics Inc., USA).

Biodistribution of iRGD-PSS@PBAE@IR780 NPs

Biodistribution of IR780 encapsulated NPs were detected in tumor-bearing mice via the in vivo imaging system. In brief, 4T1 tumor-bearing nude mice were separately intravenously injected with 100 μL of normal saline (the control group), free IR780, PSS@PBAE@IR780 and iRGD-PSS@PBAE@IR780 NPs, at the IR780 dose of 400 μg/kg and then photographed by an IVIS in vivo imaging system (PerkinElmer, USA) at 2, 8, 24 and 48 h post-injection. All the mice were then sacrificed, and the main organs and tumors were collected for further evaluation of tissue accumulation. At least three mice were used for each group.

Assessment of Intratumoral Cellular Uptakes

Intratumoral cellular uptakes of IR780 encapsulated NPs were detected in tumor-bearing mice via the fluorescence imaging technique. At 24 h after intravenous injection, the mice were then sacrificed, and then the tumors were collected for further cryo-section. Afterward, the tumor sections were stained with DAPI and then photographed by a fluorescence microscope.

Evaluation of Intratumoral Production of ROS

DCFH-DA was used as a fluorescence probe for the evaluation of intratumoral production of ROS. In brief, 4T1 tumor-bearing nude mice were separately intravenously injected with 100 μL of normal saline (the control group), free JQ1, free ORI, JQ1/ORI mixture, PSS@PBAE@JQ1/ORI and iRGD-PSS@PBAE@JQ1/ORI NPs at the JQ1 and ORI doses of 5 mg/kg, respectively. At 24 h after intravenous injection, all the mice were then intravenously injected with 50 μL DCFH-DA (20 μM). After 30 min, the mice were sacrificed, and then the tumors were collected for further section. Afterward, the tumor sections were stained with DAPI and then photographed by a fluorescence microscope.

Antitumor Efficacy of iRGD-PSS@PBAE@JQ1/ORI NPs

We further assessed the synergistic effects of iRGD-PSS@PBAE@JQ1/ORI NPs in 4T1 tumor-bearing mice. All mice were randomly divided into 6 groups with 6 mice per group. All treatments, including normal saline (the control group), free JQ1, free ORI, JQ1/ORI mixture, PSS@PBAE@JQ1/ORI and iRGD-PSS@PBAE@JQ1/ORI NPs, were given through intravenous injection every 2 days for consecutive 5 times at JQ1 and ORI doses of 5 mg/kg, respectively. Afterward, changes in tumor volumes and body weights were detected every 2 days for consecutive 20 days, and then the main tissues and tumors were harvested for histopathological and immunohistochemical detections.

The above tissue samples were fixed in 4% paraformaldehyde, embedded in paraffin, and cut into 5-μm sections. After that, sections were stained with hematoxylin and eosin (H&E) and then imaged with a fluorescence microscope. We further detected the changes of PD-L1 and Ki67 (a tumor cell proliferation-related biomarker) in tumor tissues by immunohistochemical analysis. The sections of the tumor were processed separately with primary antibody against PD-L1 and Ki67 (Abcam, Cambridge, UK) at 4°C overnight, and then incubated with secondary antibody conjugated with HRP, stained with diaminobenzidine and hematoxylin, and subsequently observed under a fluorescence microscope.

Statistical Analysis

All data were demonstrated as means ± standard deviation (SD). Statistical analysis was conducted using SPSS 20.0 software. The comparisons between the control and treatment groups were determined using the Student's *t*-test or one-way ANOVA analysis. *P* value less than 0.05 was considered to be statistically significant.

Results and Discussion

Synthesis and Chemical Characterization of iRGD-PSS@PBAE@JQ1/ORI NPs

We modified the marine sulfated polysaccharide PSS with the tumor penetrating peptide iRGD to acquire the multi-functional nanocarrier materials in this work. As shown in Scheme 1A, iRGD peptide was covalently coupled with PSS by an amidation reaction between the terminal amino groups of iRGD and the carboxyl groups of PSS. The chemical structure of iRGD-PSS was confirmed by FT-IR and ^{1}H-NMR. In the IR spectrum of iRGD-PSS (Figure 1A), the stretching vibrations of O-H and N-H corresponding, respectively, to PSS and iRGD were observed at 3300–3600 cm^{-1}. The stretching vibration of O-H was at 3400–3600 cm^{-1} in the spectrum of PSS, which included hydroxyl groups and carboxylic acid. In contrast, there was no alcoholic hydroxyl group in the structure of iRGD, and the stretching vibrations of O-H and N-H in the IR spectrum of iRGD appeared at 3300 cm^{-1}. Moreover, the characteristic amide bands I and II of iRGD were visible at 1680 and 1560 cm^{-1} in the spectra of iRGD and iRGD-PSS. The ^{1}H-NMR spectra of PSS, iRGD and iRGD-PSS are shown in Figure 1B. The proton peaks of the methyl group (1.0 ppm) from PSS were observed in the spectra of PSS and iRGD-PSS. The characteristic peaks of the guanidine group (3.09 ppm) and pyrrolidine (3.98, 3.84, 2.13 and 1.88 ppm) from iRGD peptide were visible in the spectrum of iRGD-PSS. All the above data suggested that iRGD-PSS was successfully synthesized. In addition, the graft efficiency of iRGD-PSS was 26.32%.

ssPBAE was synthesized according to our previous report[31] and confirmed by the ^{1}H-NMR method (Figure S1). Both JQ1 and ORI are water-insoluble which significantly restricts their potential therapeutic applications. Here, a facile, one-step method, the nanoprecipitation method, was used to synthesize NPs for co-loading JQ1 and ORI, and then further surface-modification with iRGD-PSS. As shown in Figure 1C, iRGD-PSS@PBAE@JQ1/ORI NPs had a clear "core-shell" structure and the particle means diameter was 162.0 ± 14.9 nm with a relatively narrow distribution (PDI was 0.142) (Figure 1D). The zeta potential of iRGD-PSS@PBAE@JQ1/ORI NPs was −46.6 mV, which demonstrated that the polyanionic iRGD-PSS as a hydrophilic nanoshell was successfully adsorbed on the surface hydrophobic ssPBAE nanocore co-loading JQ1 and ORI. The loading contents of JQ1 and ORI in iRGD-PSS@PBAE@JQ1/ORI NPs detected by HPLC were 4.75% and 7.11%, and their corresponding encapsulation efficiencies were 61.7% and 92.4%, respectively. In addition, the size and PDIs of iRGD-PSS@PBAE@JQ1/ORI NPs maintained relative stability during a 6-day storage period, exhibiting good in vitro stability, both in PBS and 10% FBS solution (Figure 1E). For comparison, PSS@PBAE@JQ1/ORI NPs without iRGD peptides were also prepared and showed a uniform and spherical shape with a slightly smaller size of about 152.0 ± 15.1 nm than iRGD-PSS@PBAE@JQ1/ORI NPs (Figure S2). Additionally, the

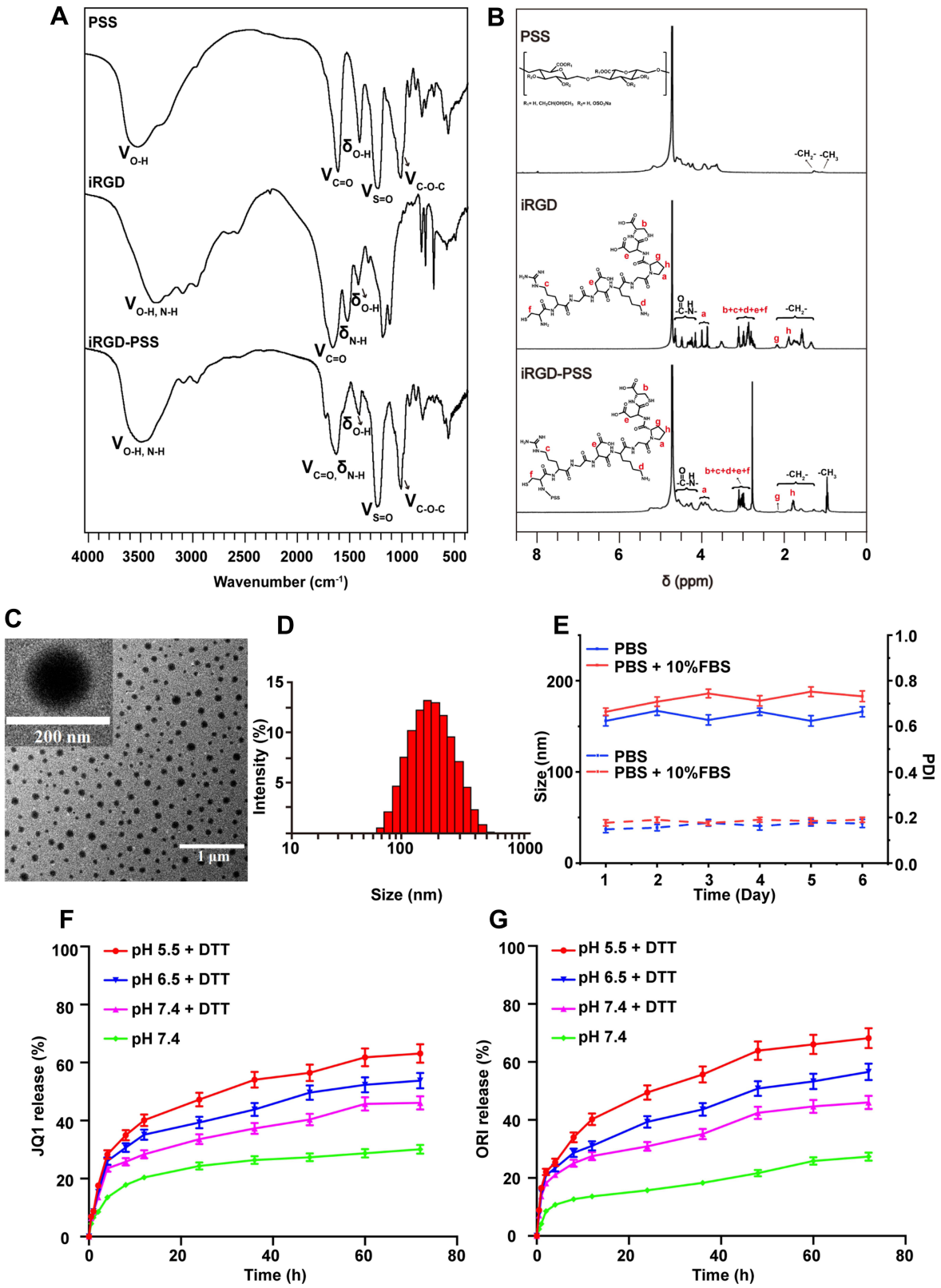

Figure 1 Characterization and properties of iRGD-PSS@PBAE@JQ1/ORI NPs in vitro. (**A**) The IR spectra of iRGD-PSS@PBAE@JQ1/ORI NPs. (**B**) The 1H-NMR spectra of iRGD-PSS@PBAE@JQ1/ORI NPs. (**C**) The morphology of iRGD-PSS@PBAE@JQ1/ORI NPs observed by the TEM. (**D**) The size distribution of iRGD-PSS@PBAE@JQ1/ORI NPs detected by the dynamic laser scattering method. (**E**) The changes of size and PDIs of iRGD-PSS@PBAE@JQ1/ORI NPs during storage in PBS supplemented with/without 10% FBS. (**F** and **G**) The releases of JQ1 (**F**) and ORI (**G**) from iRGD-PSS@PBAE@JQ1/ORI NPs in vitro at different pH values (pH 5.5, 6.5, 7.4) and with/without 10 mM DTT.

cytotoxicities of iRGD-PSS@PBAE and PSS@PBAE in breast cancer cells were evaluated by the MTT assay. The results showed that iRGD-PSS@PBAE and PSS@PBAE have no obvious cytotoxicities (Figure S4).

Releases Properties of JQ1 and ORI

Because it possesses disulfide bond and tertiary amine group in its structure repeat unit, ssPBAE shows pH and redox dual sensitives. The morphological changes of iRGD-PSS@PBAE@JQ1/ORI NPs were imaged after 24-h incubation in DTT (10 mM) solution. The iRGD-PSS@PBAE@JQ1/ORI NPs were disintegrated, and only aggregates and complex debris were observed (Figure S3). Then, we detected the release profiles of JQ1 and ORI from iRGD-PSS@PBAE@JQ1/ORI NPs at different pH values (pH 5.5, 6.5, 7.4) and with/without 10 mM DTT (Figure 1F and G). In PBS solution without adding DTT, only about 30% of JQ1 was released at 72 h. The JQ1 release rate was significantly accelerated in the release medium supplemented with DTT. Especially at pH 5.5, more than 60% of JQ1 was released from iRGD-PSS @PBAE@JQ1/ORI NPs at 72 h. ORI also exhibited pH- and redox-sensitive release behavior from iRGD-PSS @PBAE@JQ1/ORI NPs. All the above results further confirmed the pH and reductive environment dual responsive capabilities of iRGD-PSS@PBAE@JQ1/ORI NPs.

Cellular Uptakes of IR780 Encapsulated NPs

IR780 was loaded into iRGD-modified NPs to assess the cellular uptake in high $\alpha_v\beta_3$ integrin receptors-expressing 4T1 cells using the fluorescence microscopy and the flow cytometry.[17] Some of the cells were pre-incubated with free iRGD for competitively binding to the integrin receptors on the surface of 4T1 cells. Then, all the groups were incubated with free IR780, PSS@PBAE@IR780 and iRGD-PSS@PBAE@IR780 NPs for 2 h, respectively. As shown in Figure 2A, the fluorescence of IR780 was mainly located in the cytoplasm. Free IR780 displayed relatively weak fluorescence signals due to its hydrophobicity. By contrast, PSS@PBAE@IR780 and iRGD-PSS@PBAE@IR780 NPs enhanced the intracellular fluorescence signals of IR780. The iRGD-PSS@PBAE@IR780 NPs showed much stronger signals than PSS@PBAE@IR780, indicating the iRGD-mediated more endocytosis of NPs. After being pre-treated with free iRGD, the fluorescence signal of IR780 in the iRGD-PSS@PBAE@IR780 NPs group significantly decreased. The PSS@PBAE@IR780 nanoparticle group was almost unchanged, which verified the specific receptor-mediated endocytosis. The flow cytometry analysis further confirmed that the cellular uptake efficiency of iRGD-PSS@PBAE@IR780 NPs was significantly higher than that of PSS@PBAE@IR780 (Figure 2B). From the above results, we deduced that iRGD surface-modified NPs could realize the efficient delivery of antitumor drugs into tumor cells.

Penetration of IR780 Encapsulated NPs into Breast Tumor-Like Spheroids

To investigate whether iRGD-modified NPs could further enhance their penetration into tumor interiors, we constructed 3D spheroids of breast cancer 4T1 cells. After 2, 6, 12 h incubated with free IR780, PSS@PBAE@IR780 and iRGD-PSS @PBAE@IR780 NPs, the 3D tumor-like spheroids were observed under the confocal microscopy (Figure 2C). The fluorescence signals of free IR780 and PSS@PBAE@IR780 NPs were observed only at the margins of tumor spheroids, even after 12-h incubation. In contrast, the iRGD-PSS@PBAE@IR780 NPs had a rapid penetration speed, and penetrated deeper, and distributed more extensively in the whole tumor spheroids. The subsequent values of the relative fluorescence areas (RFAs) of IR780 were consistent with confocal images. The iRGD-PSS@PBAE@IR780 NPs were higher than free IR780 and PSS@PBAE@IR780 NPs at 12 h (Figure 2D). These results revealed that iRGD peptide enhanced the NPs' tumor-penetrating abilities and could mediate more efficient drug delivery to the tumor interior.

Cytotoxicity of iRGD-PSS@PBAE@JQ1/ORI NPs in Breast Cancer Cells

We evaluated the cytotoxicity of iRGD-PSS@PBAE@JQ1/ORI NPs in breast cancer cells by the MTT assay. After incubation for 24/48 h, both free JQ1 and ORI exhibited cytotoxicity in a dose-dependent manner, and their IC_{50} were approximately 10.1 and 5.2 μg/mL (24 h), 2.5 and 1.8 μg/mL (48 h), respectively. As shown in Figure 3A and B, the PSS@PBAE@JQ1/ORI and iRGD-PSS@PBAE@JQ1/ORI NPs showed higher cytotoxicity than free drugs, in which the IC_{50} of PSS@PBAE@JQ1/ORI and iRGD-PSS@PBAE@JQ1/ORI NPs decreased to 2.50 and 1.51 μg/mL of JQ1 (24 h), and decreased to 0.82 and 0.69 μg/mL of JQ1 (48 h). Compared to PSS@PBAE@JQ1/ORI NPs, iRGD-PSS

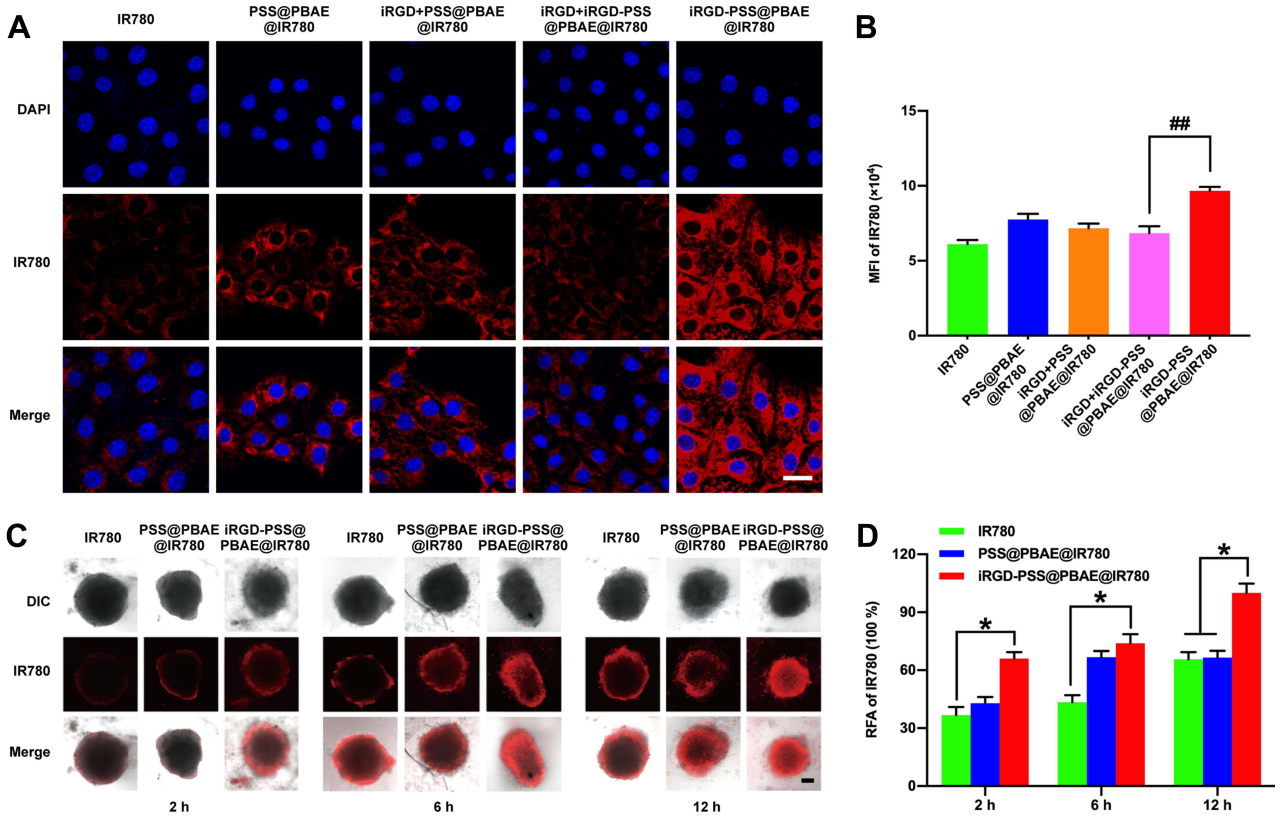

Figure 2 Cellular uptakes and penetrating ability of IR780 encapsulated NPs. (**A**) Confocal images of the cells after incubation with free IR780, PSS@PBAE@IR780 and iRGD-PSS@PBAE@IR780 NPs for 2 h (Scale bar: 20 μm). (**B**) Quantitative analyses of intracellular IR780. (**C**) Confocal images of 4T1 tumor-like spheroids after 2-hour, 6-hour and 12-hour incubation with free IR780, PSS@PBAE@IR780 and iRGD-PSS@PBAE@IR780 NPs (Scale bar: 100 μm). (**D**) Relative fluorescence areas (RFAs) of IR780 in 4T1 tumor spheroids after various treatments. $^{\#\#}$P<0.01 between two treatment groups. *P<0.05 for comparison with the IR780 group.

@PBAE@JQ1/ORI NPs displayed slightly higher cytotoxicity at the same JQ1 and ORI concentrations. The CI value was approximately 0.44 (<1) at 24 h, and 0.66 (<1) at 48 h. These results suggested that iRGD-PSS@PBAE@JQ1/ORI NPs could effectively deliver JQ1 and ORI into 4T1 cells, thus exerting synergistic antitumor activities.

Then, we used the LIVE/DEAD cell staining kit to visualize the synergistic cell-killing effect of iRGD-PSS @PBAE@JQ1/ORI NPs mentioned above. As shown in Figure 3C, the live and dead cells after various treatments emitted green and red fluorescence, respectively. Free JQ1, free ORI and PSS@PBAE@JQ1/ORI NPs induced most of the cell's death, and furthermore iRGD-PSS@PBAE@JQ1/ORI NPs showed stronger cell-killing effect than free JQ1, free ORI and PSS@PBAE@JQ1/ORI (Figure 3C). We also determined the apoptosis-inducing effects of iRGD-PSS @PBAE@JQ1/ORI NPs on 4T1 cells using flow cytometry. As shown in Figure 3D, free JQ1 and free ORI exhibited moderate apoptosis induction effects after 24 h treatments. JQ1/ORI mixture and PSS@PBAE@JQ1/ORI NPs significantly induced early and late-stage apoptosis. Moreover, iRGD-PSS@PBAE@JQ1/ORI NPs exhibited much stronger apoptosis-inducing effects than other treatments, especially early-stage apoptosis (42.5%), and only 23.3% of the cells were alive after 24-h treatment. Accordingly, we deduced that iRGD-PSS@PBAE@JQ1/ORI NPs could realize the synergistic effects against tumor cells.

Evaluation of iRGD-PSS@PBAE@JQ1/ORI NPs on Intracellular ROS Production

Cytotoxic ROS production is one of the main anti-cancer mechanisms of ORI. DCFH-DA was applied as a fluorescence probe for the detection of intracellular ROS production, thus evaluating the iRGD-PSS@PBAE@JQ1/ORI NPs anticancer efficacy. The cells treated with iRGD-PSS@PBAE@JQ1/ORI NPs had stronger fluorescence intensity than other groups, indicating more ORI was mediated by iRGD-PSS@PBAE@JQ1/ORI NPs to enter the cells (Figure 4A). The intracellular ROS levels were also quantitatively detected by flow cytometry, and similar results were obtained

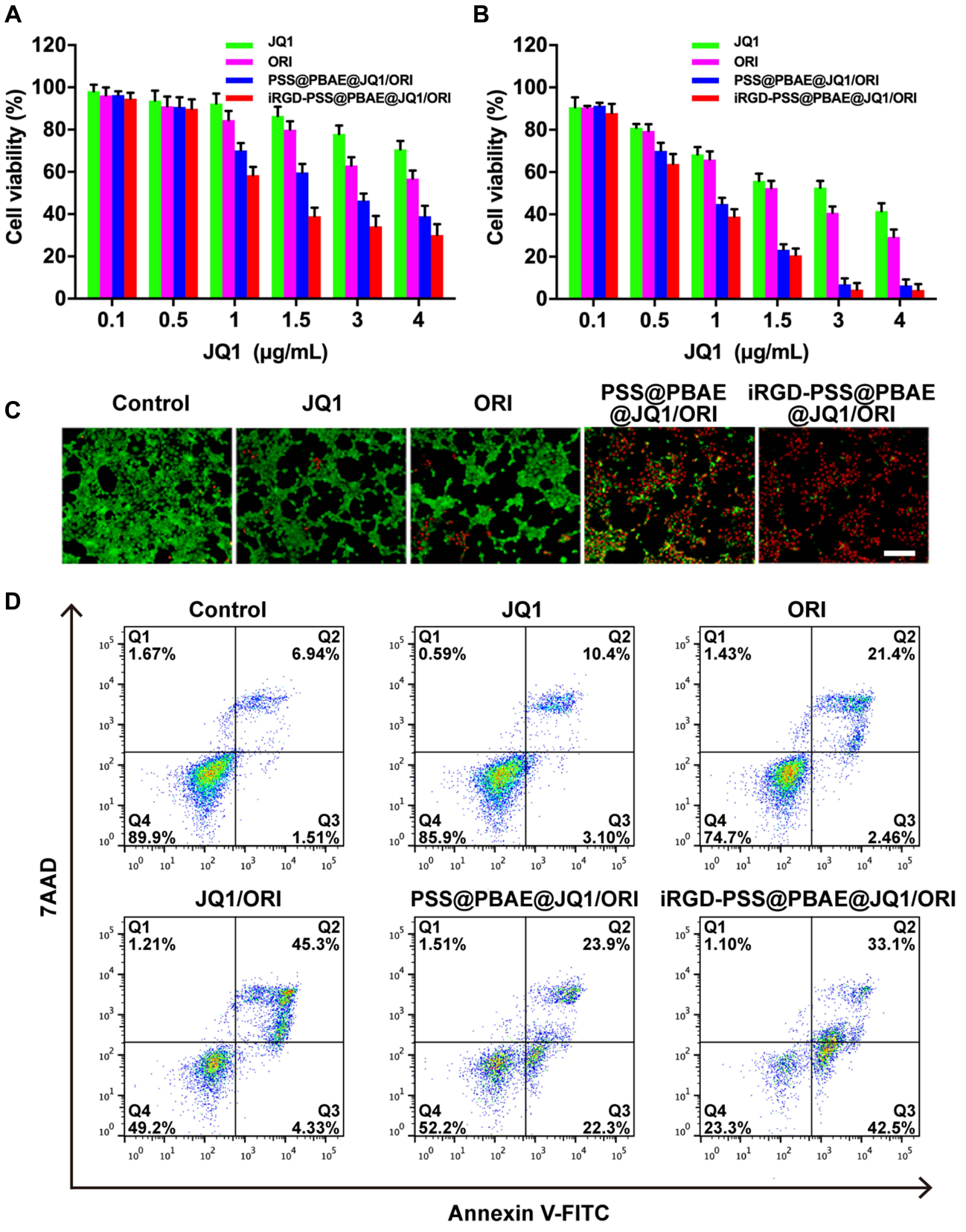

Figure 3 Inhibition of iRGD-PSS@PBAE@JQ1/ORI NPs on the growth of breast cancer cells. The cytotoxicities of free JQ1, ORI, PSS@PBAE@JQ1/ORI and iRGD-PSS @PBAE@JQ1/ORI NPs in 4T1 cells after 24-hour treatments (**A**) and 48-hour treatments (**B**) at different JQ1 concentrations. (**C**) The LIVE/DEAD analysis of cells at 24 h after various treatments (Scale bar: 200 μm). (**D**) Cell apoptosis was quantified by flow cytometry at 24 h after various treatments (Q1: dead cells; Q2: late apoptotic cells; Q3: early apoptotic cells; Q4: live cells).

https://doi.org/10.2147/IJN.S343902 DovePress

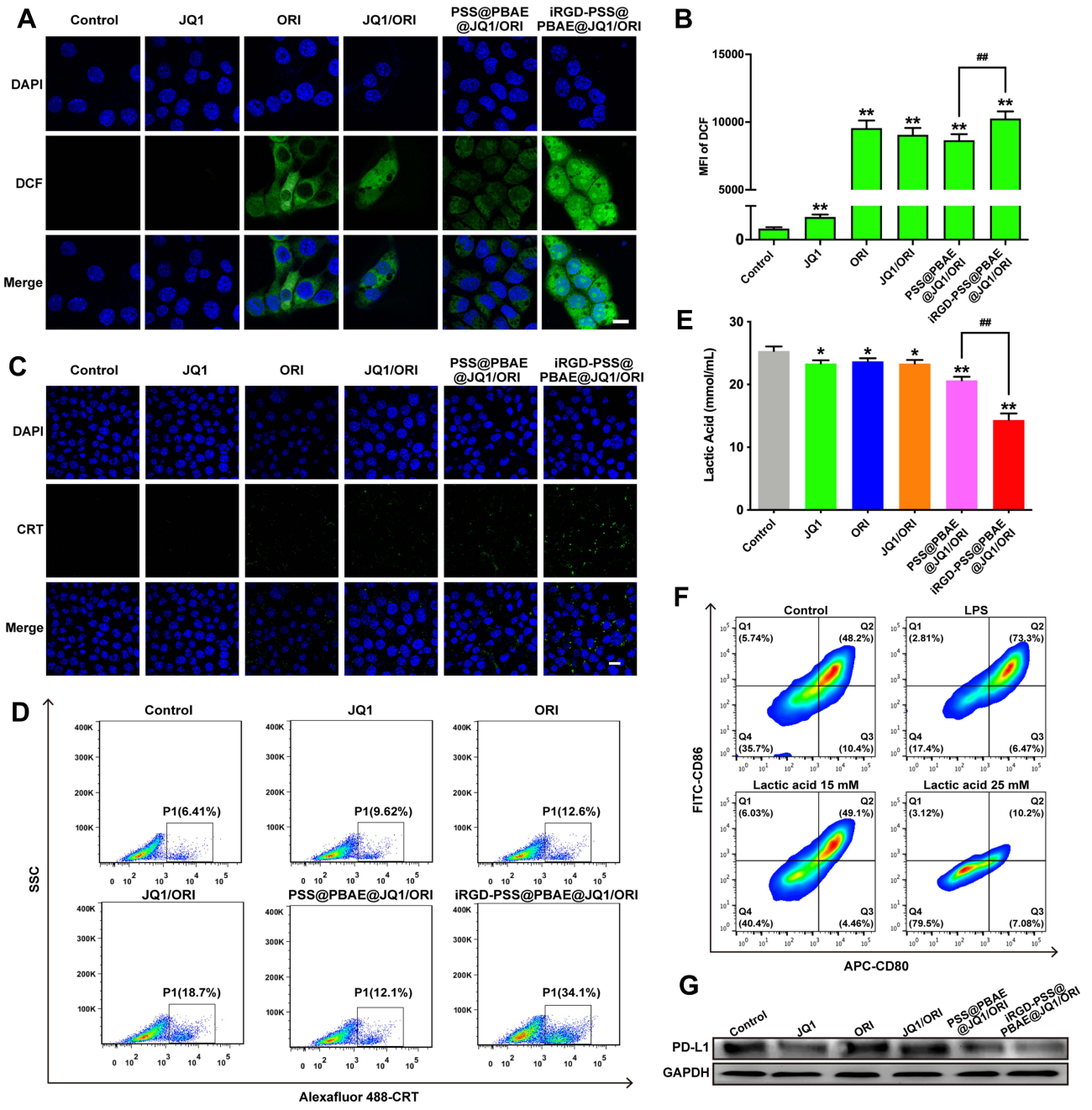

Figure 4 Effects of iRGD-PSS@PBAE@JQ1/ORI NPs on the production of intracellular ROS, ICD-induced immune priming and lactic acid secretion. The confocal images (**A**) and the flow cytometric analysis (**B**) of intracellular ROS productions in 4T1 cells at 24 h after various treatments (Scale bar: 20 μm). The confocal images (**C**) and the flow cytometric analysis (**D**) of CRT exposure levels in 4T1 cells at 24 h after various treatments (Scale bar: 20 μm). (**E**) The production of lactic acid in 4T1 cells at 24 h after various treatments. (**F**) The flow cytometric analysis of inhibition on DC maturation at 24 h after various treatments. (**G**) PD-L1 expression in 4T1 cells after various treatments. $^{\#\#}$P<0.01 between two treatment groups. *P<0.05 and **P<0.01 for comparison with the control group.

(Figure 4B). As described above, the iRGD-PSS@PBAE@JQ1/ORI NPs displayed a more potent ROS generation effect due to the enhanced cellular internalization of ORI by iRGD-modified NPs.

Effect of iRGD-PSS@PBAE@JQ1/ORI NPs on ICD-Induced Immune Priming

Immunogenic cell death (ICD) of tumor cells plays an important role in priming antitumor immune response. The exposure of CRT to the surface of cancer cells, as one of the danger signals induced by ICD, could be recognized by antigen-presentation cells and further enhanced the proliferation of CTLs. ICD could be evoked through ROS production

via endoplasmic reticulum stress. Accumulated studies have shown that natural products could serve as ICD-triggers and consequently elicit antitumor immunity.[17] Based on the potent effects of intracellular ROS generation and cytotoxicity, we deduced that iRGD-PSS@PBAE@JQ1/ORI NPs could induce ICD. The cells treated with free ORI slightly exhibited CRT exposure, owing to the ROS generation (Figure 4C). In addition, the iRGD-PSS@PBAE@JQ1/ORI NPs significantly increased the exposure level of CRT compared to other treatment groups, in which the results were observed either by confocal images or by flow cytometry (Figure 4D). Thus, the iRGD-PSS@PBAE@JQ1/ORI NPs had the potential of immune priming via inducing ICD.

Effect of iRGD-PSS@PBAE@JQ1/ORI NPs on Lactic Acid Secretion

Lactic acid is a major product of glucose metabolism in cancer cells, leading to immunosuppressive TME and inhibition of dendritic-cells (DCs) differentiation. ORI can suppress cancer glucose metabolism and reduce the lactic acid export from tumor cells. Hence, we investigated the secretion levels of lactic acid of 4T1 cells after various treatments and whether the lactic acid could influence the maturation of BMDCs in vitro. As shown in Figure 4E, after being treated with iRGD-PSS@PBAE@JQ1/ORI NPs, the production of lactic acid in 4T1 cells significantly reduced to 14.3 mM, while the value of the control group was nearly 25 mM. The flow cytometry results demonstrated that a relatively higher concentration of lactic acid (25 mM) could remarkably inhibit DCs maturation, while the lower concentration of lactic acid (15 mM) could relieve the inhibition (Figure 4F). We also used Western blots to analyze the PD-L1 downregulation mediated by JQ1. Remarkable downregulation of PD-L1 protein was found in the 4T1 cells treated with free JQ1, PSS@PBAE@JQ1/ORI, and iRGD-PSS@PBAE@JQ1/ORI NPs. Notably, the cells treated with iRGD-PSS @PBAE@JQ1/ORI NPs decreased the most (Figure 4G). All these results suggested that iRGD-PSS@PBAE@JQ1/ ORI NPs could reduce lactic acid production.

In vivo Biodistribution and Tumor Accumulation Studies of IR780 Encapsulated NPs

To assess the tumor-targeting capability of iRGD-modified NPs, we used IR780 encapsulated NPs to investigate the biodistribution and tumor accumulation in tumor-bearing mice. Figure 5A shows the fluorescence images of mice at 2, 8, 24, and 48 h after administrations of normal saline, free IR780, PSS@PBAE@IR780 and iRGD-PSS@PBAE@IR780 NPs. Compared to free IR780 and PSS@PBAE@IR780 NPs, the iRGD-PSS@PBAE@IR780 NPs showed an evident tumor distribution at 8 h. They significantly increased tumor accumulation at 24 h and 48 h after intravenous injection, indicating their good tumor-targeting abilities through both the passive EPR effect and the active ligand-receptor binding manner. Afterward, the major organs and tumor tissues were collected for further imaging. The results are shown in Figure 5B and C. At 48 h after administration, free IR780 was mainly metabolized, and only weak fluorescent signals were observed. By contrast, the PSS@PBAE@IR780 and iRGD-PSS@PBAE@IR780 NPs displayed fluorescent signals in the tumor, liver, lung and kidney. However, the iRGD-PSS@PBAE@IR780 NPs showed enhanced tumor accumulation and reduced lung, kidney and liver distribution compared to PSS@PBAE@IR780 NPs. All the above results indicated that the iRGD mediated the active targeting effect that enhanced the tumor accumulation of NPs,while it reduced the distribution in normal tissues.

Intratumoral Localization and ROS Generation Efficacy of iRGD-PSS@PBAE@JQ1/ ORI NPs in Tumor-Bearing Mice

The intratumoral localization and ROS generation efficacy of iRGD-PSS@PBAE@JQ1/ORI NPs were assessed in tumor-bearing mice. First, we observed the intratumoral localization of iRGD-PSS@PBAE@IR780 NPs in tumor-bearing mice. The confocal images of tumor sections derived from the mice at 24 h after intravenous injections of free IR780, PSS@PBAE@IR780 and iRGD-PSS@PBAE@IR780 NPs are shown in Figure 5D. Free IR780 was mostly located in the intercellular space due to its poor cell-entry ability. However, IR780 loaded by PSS@PBAE@IR780 and iRGD-PSS@PBAE@IR780 was significantly internalized into tumor cells. This tumor cell-targeting property would be very favorable for iRGD exerting its active tumor-targeting capability.

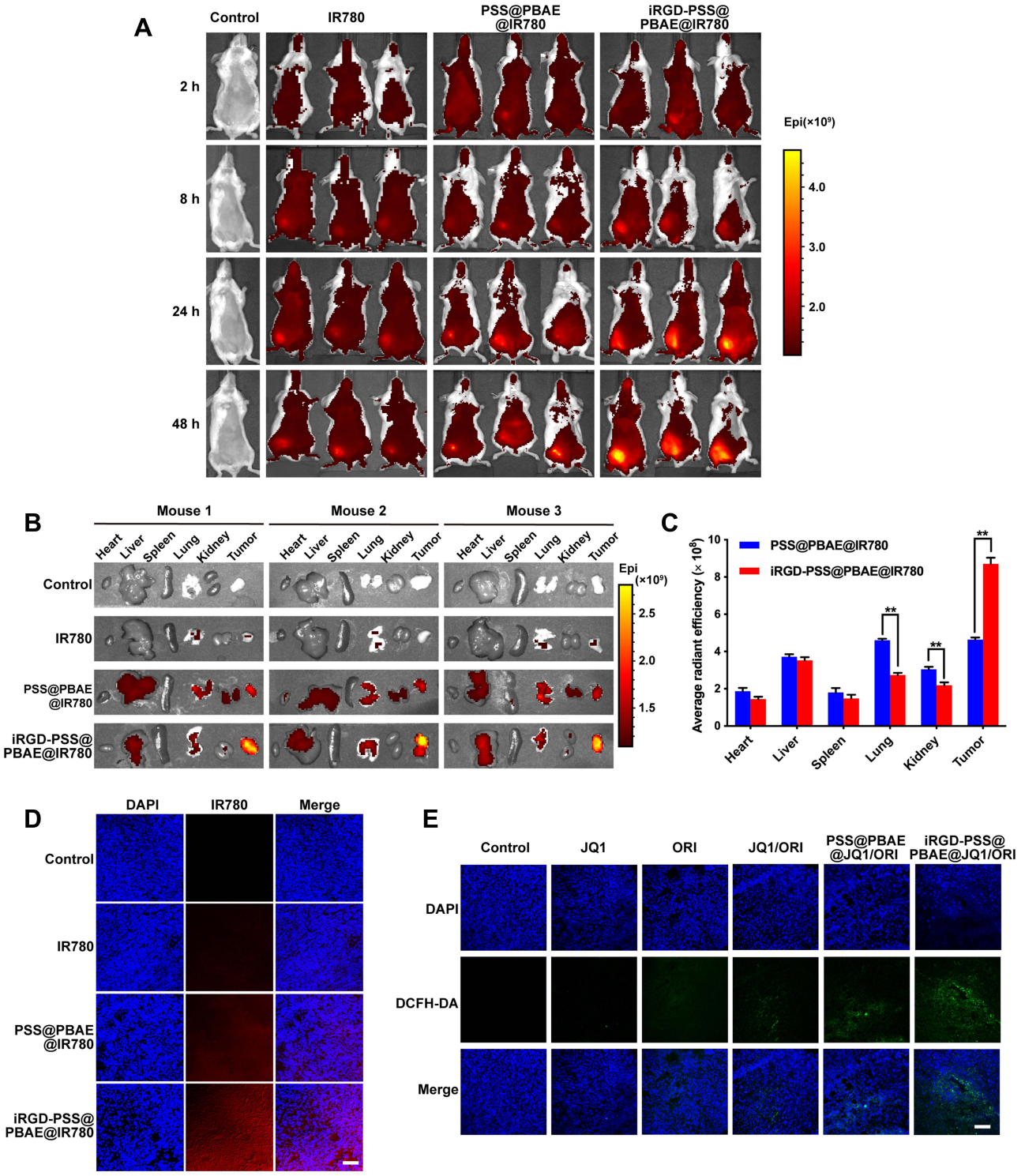

Figure 5 Biodistribution and tumor accumulation studies in 4T1 tumor-bearing mice. (**A**) The in vivo imaging photos of mice at different times after administrations. Tissue distribution and tumor-accumulation of IR780 encapsulated NPs in 4T1 tumor-bearing mice. (**B**) The fluorescent images of major organs and tumor tissues were removed from the mice at 48 h after intravenous injections of normal saline (the control), free IR780, PSS@PBAE@IR780 and iRGD-PSS@PBAE@IR780 NPs. (**C**) The comparisons of chemiluminescence image's average radiant efficiency detected from major organs and tumor tissues at 48 h after administrations. ** indicate P<0.01 for comparison with the PSS@PBAE@IR780 NPs group. (**D**) The confocal images of intratumoral localization of IR780 encapsulated NPs at 24 h after various treatments. (**E**) The confocal images of intratumoral ROS generation after various treatments (Scale bar: 100 μm).

The confocal images of DCFH-DA-processed tumor sections derived from the mice with different fluorescence intensities are shown Figure 5E. Compared to the control, the intratumoral fluorescence intensities in other treatment groups were enhanced, indicating that these treatments promoted the productions of large amounts of ROS. However, iRGD-PSS@PBAE@JQ1/ORI exhibited greater ROS generation efficiencies than PSS@PBAE@JQ1/ORI owing to more efficient cellular internalization through the mediation of iRGD.

Antitumor Efficacy of iRGD-PSS@PBAE@JQ1/ORI NPs in Tumor-Bearing Mice

The antitumor efficacy of iRGD-PSS@PBAE@JQ1/ORI NPs was evaluated in tumor-bearing mice. The curves of tumor growth are shown in Figure 6A. Free JQ1, free ORI and JQ1/ORI mixture exhibited no significant inhibitory effect on tumor growth. Compared to the above treatments, PSS@PBAE@JQ1/ORI and iRGD-PSS@PBAE@JQ1/ORI NPs showed potent tumor-inhibitory activity, indicating that the NPs facilitated the delivery of therapeutic drugs. More importantly, iRGD-PSS @PBAE@JQ1/ORI NPs showed a much stronger tumor-inhibitory effect than PSS@PBAE@JQ1/ORI NPs. As shown in

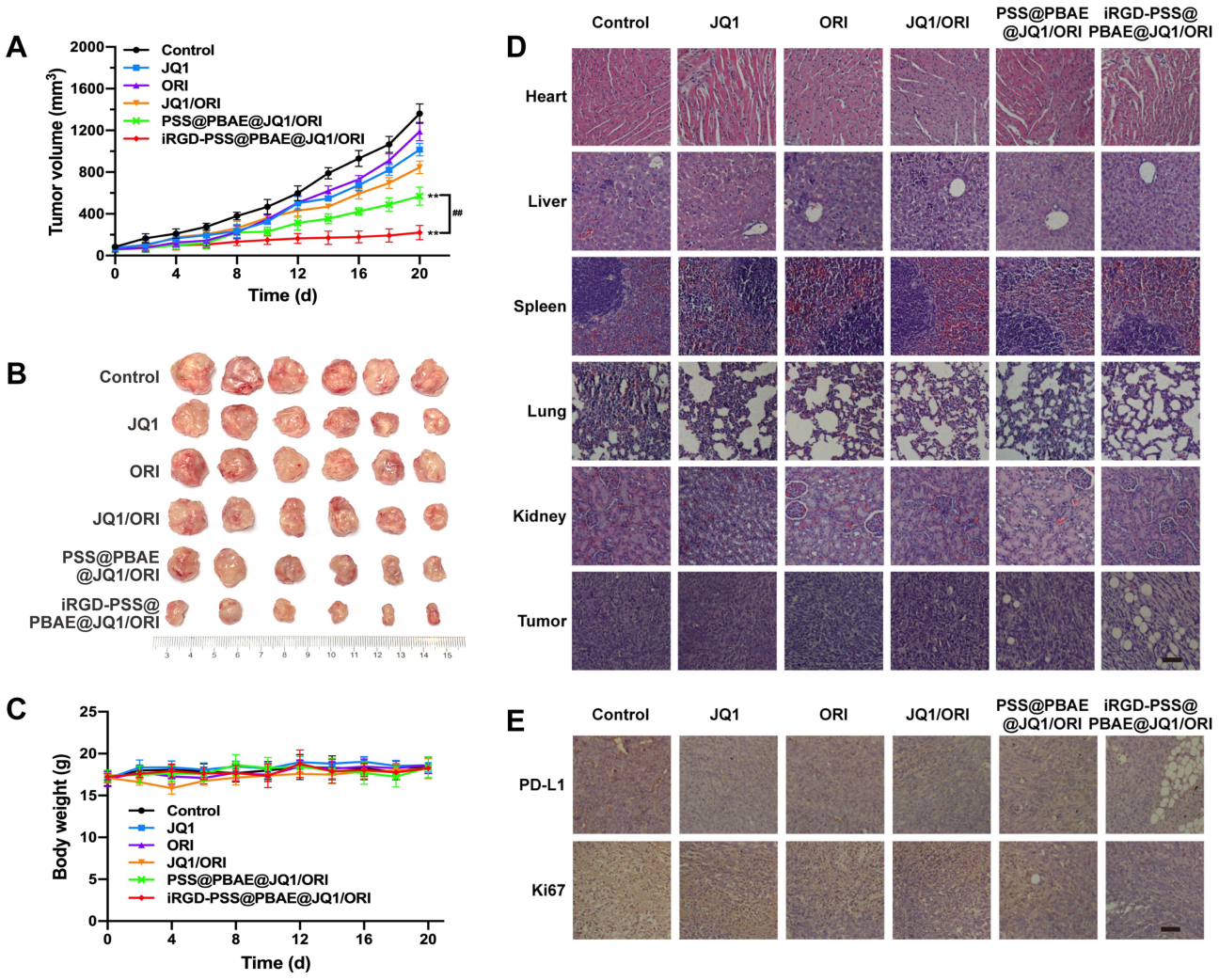

Figure 6 Inhibition of iRGD-PSS@PBAE@JQ1/ORI NPs on the growth of breast cancer in 4T1 tumor-bearing mice. The curves of tumor growth (**A**) and the photograph of tumors (**B**) in the mice with treatments of normal saline (the control), JQ1, ORI, JQ1/ORI mixture, PSS@PBAE@JQ1/ORI and iRGD-PSS@PBAE@JQ1/ORI NPs. (**C**) The changes of mouse body weights during the whole treatment period. (**D**) The microscopic images of H&E stained sections of tumors and major organs were removed from the mice with different treatments (Scale bar: 100 μm). (**E**) The microscopic images of tumor sections with staining of PD-L1 and Ki67 (Scale bar: 100 μm). $^{\#\#}$P<0.01 between two treatment groups. **P<0.01 for comparison with the control group.

Figure 6B, the iRGD-PSS@PBAE@JQ1/ORI NPs treatment group's tumors were much smaller than those in the other treatment groups. It could be deduced that the abilities of tumor targeting, tissue penetrating, and controlled release would help the iRGD-PSS@PBAE@JQ1/ORI NPs efficiently deliver JQ1 and ORI to the tumor cells, thus exerting the synergistic antitumor efficacy. In addition, no obvious changes in body weights of the mice were observed in all these treatment groups, which demonstrated that these treatments had no obvious side and toxic effects (Figure 6C).

The H&E staining pictures of the tumor and main organs sections are shown in Figure 6D. No pathological changes were observed in sections of major organs compared to the control group. However, the necrosis phenomenon was observed in the tumor section in mice treated with iRGD-PSS@PBAE@JQ1/ORI NPs. Moreover, lung metastasis occurred in the mice of the control group but was almost disappeared in the mice of the iRGD-PSS@PBAE@JQ1/ORI NPs group. Hence, we believed that the iRGD-PSS@PBAE@JQ1/ORI NPs could suppress the lung metastasis due to PSS and ORI's antiangiogenic ability. Figure 6E shows the microscopic images of tumor sections stained with antibodies against PD-L1 and Ki67. The PD-L1 expression was downregulated in the tumor section treated with iRGD-PSS@PBAE@JQ1/ORI NPs. Moreover, the tumor proliferation-associated antigen Ki67 was also downregulated in the treatment group of iRGD-PSS@PBAE@JQ1/ORI NPs, indicating that the iRGD-PSS@PBAE@JQ1/ORI NPs could significantly inhibit tumor cell proliferation compared with other treatment groups. All these results further proved the synergistic antitumor efficacy based on iRGD-PSS@PBAE@JQ1/ORI NPs.

Conclusions

In this study, we successfully prepared an iRGD tumor-penetrating peptide-modified nanotherapeutic system based on a marine sulfated polysaccharide PSS against breast cancer via co-loading of JQ1 and ORI. The iRGD-PSS @PBAE@JQ1/ORI NPs exhibited pH and redox-dual responsive release of therapeutic drugs owing to ssPBAE. In vitro and in vivo, the iRGD-modified NPs significantly improved the cellular internalization and tumor penetration through the mediation by the iRGD peptide. The results revealed iRGD-PSS@PBAE@JQ1/ORI NPs achieved significant synergistic effects evolved multi-mechanisms including downregulation PD-L1, ROS generation and antiproliferation, etc. Altogether, these multifunctional nanotherapeutic systems provided a novel strategy combining JQ1 and ORI, which exhibited great potential for the clinical therapy of breast cancer.

Acknowledgments

This work was supported by the Science & Technology Development Fund of Tianjin Education Commission for Higher Education (Grant No. 2019KJ179).

Disclosure

The authors report no conflicts of interest in this work.

References

1. Siegel RL, Miller KD, Fuchs HE, Jemal A. Cancer statistics, 2021. *CA Cancer J Clin*. 2021;71(1):7–33. doi:10.3322/caac.21654
2. Deepak KGK, Vempati R, Nagaraju GP, et al. Tumor microenvironment: challenges and opportunities in targeting metastasis of triple negative breast cancer. *Pharmacol Res*. 2020;153:104683. doi:10.1016/j.phrs.2020.104683
3. Shi J, Liu F, Song Y. Progress: targeted therapy, immunotherapy, and new chemotherapy strategies in advanced triple-negative breast cancer. *Cancer Manag Res*. 2020;12:9375–9387. doi:10.2147/CMAR.S272685
4. Dalum GV, Stam G, Tibbe A, Franken B, Terstappen L. Circulating tumor cells before and during follow-up after breast cancer surgery. *Int J Oncol*. 2014;46(1):407–413. doi:10.3892/ijo.2014.2694
5. Liyanage PY, Hettiarachchi SD, Zhou Y, et al. Nanoparticle-mediated targeted drug delivery for breast cancer treatment. *Biochim Biophys Acta Rev Cancer*. 2019;1871(2):419–433. doi:10.1016/j.bbcan.2019.04.006
6. Li P, Hao J, Li H, Guan H, Li C. Development of an enteric nanoparticle of marine sulfated polysaccharide propylene glycol alginate sodium sulfate for oral administration: formulation design, pharmacokinetics and efficacy. *J Pharm Pharmacol*. 2018;70(6):740–748. doi:10.1111/jphp.12902
7. Gao Y, Zhang L, Jiao W. Marine glycan-derived therapeutics in China. *Prog Mol Biol Transl Sci*. 2019;163:113–134. doi:10.1016/bs.pmbts.2019.02.006
8. Shan M, Feng N, Zhang L. Efficacy of heparinoid PSS in treating cardiovascular diseases and beyond-A review of 31 years clinical experiences in China. *Prog Mol Biol Transl Sci*. 2019;163:75–93. doi:10.1016/bs.pmbts.2019.02.007
9. Mao Y, Hu Y, Feng W, et al. Effects and mechanisms of PSS-loaded nanoparticles on coronary microcirculation dysfunction in streptozotocin-induced diabetic cardiomyopathy rats. *Biomed Pharmacother*. 2020;121:109280. doi:10.1016/j.biopha.2019.109280

10. Zhang T, Liu H, Li Y, et al. A pH-sensitive nanotherapeutic system based on a marine sulfated polysaccharide for the treatment of metastatic breast cancer through combining chemotherapy and COX-2 inhibition. *Acta Biomater*. 2019;99:412–425. doi:10.1016/j.actbio.2019.09.001
11. Niu Y, Zhu J, Li Y, et al. Size shrinkable drug delivery nanosystems and priming the tumor microenvironment for deep intratumoral penetration of nanoparticles. *J Control Release*. 2018;277:35–47. doi:10.1016/j.jconrel.2018.03.012
12. Lv L, Shi Y, Wu J, Li G. Nanosized drug delivery systems for breast cancer stem cell targeting. *Int J Nanomedicine*. 2021;16:1487–1508. doi:10.2147/IJN.S282110
13. Erel-Akbaba G, Carvalho LA, Tian T, et al. Radiation-induced targeted nanoparticle-based gene delivery for brain tumor therapy. *ACS Nano*. 2019;13(4):4028–4040. doi:10.1021/acsnano.8b08177
14. Le TD, Nakagawa O, Fisher M, Juliano RL, Yoo H. RGD conjugated dendritic polylysine for cellular delivery of antisense oligonucleotide. *J Nanosci Nanotechnol*. 2017;17(4):2353–2357. doi:10.1166/jnn.2017.13335
15. Wang K, Zhang X, Liu Y, Liu C, Jiang B, Jiang Y. Tumor penetrability and anti-angiogenesis using iRGD-mediated delivery of doxorubicin-polymer conjugates. *Biomaterials*. 2014;35(30):8735–8747. doi:10.1016/j.biomaterials.2014.06.042
16. Jiang Y, Pang X, Liu R, et al. Design of an amphiphilic irgd peptide and self-assembling nanovesicles for improving tumor accumulation and penetration and the photodynamic efficacy of the photosensitizer. *ACS Appl Mater Interfaces*. 2018;10(37):31674–31685. doi:10.1021/acsami.8b11699
17. Hu C, Yang X, Liu R, et al. Coadministration of iRGD with multistage responsive nanoparticles enhanced tumor targeting and penetration abilities for breast cancer therapy. *ACS Appl Mater Interfaces*. 2018;10(26):22571–22579. doi:10.1021/acsami.8b04847
18. Wang P, Wang X, Luo Q, et al. Fabrication of red blood cell-based multimodal theranostic probes for second near-infrared window fluorescence imaging-guided tumor surgery and photodynamic therapy. *Theranostics*. 2019;9(2):369–380. doi:10.7150/thno.29817
19. Qiao H, Chen X, Wang Q, et al. Tumor localization of oncolytic adenovirus assisted by pH-degradable microgels with JQ1-mediated boosting replication and PD-L1 suppression for enhanced cancer therapy. *Biomater Sci*. 2020;8(9):2472–2480. doi:10.1039/d0bm00172d
20. Chen L, Zhong X, Cao W, et al. JQ1 as a BRD4 inhibitor blocks inflammatory pyroptosis-related acute colon injury induced by LPS. *Front Immunol*. 2021;12:609319. doi:10.3389/fimmu.2021.609319
21. Choi HI, An GY, Baek M, et al. BET inhibitor suppresses migration of human hepatocellular carcinoma by inhibiting SMARCA4. *Sci Rep*. 2021;11(1):11799. doi:10.1038/s41598-021-91284-2
22. Liu H, Zhang J, Quan L, et al. Conventional treatments cannot improve outcomes of early-stage primary breast marginal zone lymphoma. *Front Oncol*. 2020;10:609512. doi:10.3389/fonc.2020.609512
23. Quezada E, Cappelli C, Diaz I, et al. BET bromodomain inhibitors PFI-1 and JQ1 are identified in an epigenetic compound screen to enhance C9ORF72 gene expression and shown to ameliorate C9ORF72-associated pathological and behavioral abnormalities in a C9ALS/FTD model. *Clin Epigenetics*. 2021;13(1):56. doi:10.1186/s13148-021-01039-z
24. Wang Y, Du C, Zhao Y, Nie G, Yang Y. Trap and kill strategy for non-BRCA mutant pancreatic cancer by co-delivery of olaparib and JQ1 with plectin-1 targeting peptide nanoparticles. *Nano Today*. 2020;33:100877. doi:10.1016/j.nantod.2020.100877
25. Shu S, Lin CY, He HH, et al. Response and resistance to BET bromodomain inhibitors in triple-negative breast cancer. *Nature*. 2016;529(7586):413–417. doi:10.1038/nature16508
26. Chai D, Hao B, Hu R, et al. Delivery of oridonin and methotrexate via PEGylated graphene oxide. *ACS Appl Mater Interfaces*. 2019;11(26):22915–22924. doi:10.1021/acsami.9b03983
27. Wang Y, Zhu Z. Oridonin inhibits metastasis of human ovarian cancer cells by suppressing the mTOR pathway. *Arch Med Sci*. 2019;15(4):1017–1027. doi:10.5114/aoms.2018.77068
28. Zhao X, Zhang Q, Wang Y, et al. Oridonin induces autophagy-mediated cell death in pancreatic cancer by activating the c-Jun N-terminal kinase pathway and inhibiting phosphoinositide 3-kinase signaling. *Ann Transl Med*. 2021;9(13):1084. doi:10.21037/atm-21-2630
29. Du Y, Zhang J, Yan S, et al. Oridonin inhibits the proliferation, migration and invasion of human osteosarcoma cells via suppression of matrix metalloproteinase expression and STAT3 signalling pathway. *J BUON*. 2019;24(3):1175–1180.
30. Luo D, Yi Y, Peng K, et al. Oridonin derivatives as potential anticancer drug candidates triggering apoptosis through mitochondrial pathway in the liver cancer cells. *Eur J Med Chem*. 2019;178:365–379. doi:10.1016/j.ejmech.2019.06.006
31. Zhang S, Wang D, Li Y, et al. pH- and redox-responsive nanoparticles composed of charge-reversible pullulan-based shells and disulfide-containing poly(ss-amino ester) cores for co-delivery of a gene and chemotherapeutic agent. *Nanotechnology*. 2018;29(32):325101. doi:10.1088/1361-6528/aac4b5
32. Song H, Huang P, Niu J, et al. Injectable polypeptide hydrogel for dual-delivery of antigen and TLR3 agonist to modulate dendritic cells in vivo and enhance potent cytotoxic T-lymphocyte response against melanoma. *Biomaterials*. 2018;159:119–129. doi:10.1016/j.biomaterials.2018.01.004
33. Wan G, Cheng Y, Song J, et al. Nucleus-targeting near-infrared nanoparticles based on TAT peptide-conjugated IR780 for photo-chemotherapy of breast cancer. *Chem Eng J*. 2020;380:122458. doi:10.1016/j.cej.2019.122458
34. Shi S, Zhang L, Zhu M, et al. Reactive oxygen species-responsive nanoparticles based on PEGlated prodrug for targeted treatment of oral tongue squamous cell carcinoma by combining photodynamic therapy and chemotherapy. *ACS Appl Mater Interfaces*. 2018;10(35):29260–29272. doi:10.1021/acsami.8b08269